

Highlights

B-BACN: Bayesian Boundary-Aware Convolutional Network for Defect Characterization

Rahul Rathnakumar, Yutian Pang, Yongming Liu

- We propose a Bayesian Boundary-Aware Convolutional Network for crack segmentation.
- B-BACN decomposes uncertainty into an epistemic and aleatoric component and uses boundary refinement loss for improved crack morphology detection.
- Uncertainty formulation can aid inspection protocols by providing indicators of distribution shift and lack of training data.
- B-BACN significantly improves detection performance, reduces uncertainty, and improves expected calibration error compared to the baseline model.
- Results showed an increase in model uncertainty and a decrease in calibration with out-of-distribution samples.

B-BACN: Bayesian Boundary-Aware Convolutional Network for Defect Characterization

Rahul Rathnakumar^a, Yutian Pang^a, Yongming Liu^{a,*}

^a*School for Engineering of Matter, Transport and Energy, Arizona State University, Tempe, 85287, AZ, USA*

Abstract

Detecting accurate crack boundaries is important for condition monitoring, prognostics, and maintenance scheduling. In this work, we propose a Bayesian Boundary-Aware Convolutional Network (B-BACN) to tackle this problem, that emphasizes the importance of both uncertainty quantification and boundary refinement for producing accurate and trustworthy detections of defect boundaries. We formulate the inspection model using multi-task learning: the epistemic uncertainty is learned using Monte Carlo Dropout, and the model also learns to predict each sample's aleatoric uncertainty. A boundary refinement loss is added to improve the determination of defect boundaries. Experimental results demonstrate the effectiveness of the proposed method in accurately identifying crack boundaries, reducing misclassification and enhancing model calibration.

Keywords: Uncertainty Quantification, Defect Detection, Boundary Refinement, Convolutional Neural Network, Bayesian Deep Learning

1. Introduction

Vision-based machine learning techniques have been used in a diverse range of fields, and this paper focuses on using vision-based inspection for crack detection. The primary drivers of improvements to industrial inspection technology are higher computational power, miniaturized, commercially available sensors, and rapid advancements in machine learning techniques.

*Corresponding author.

Email address: Yongming.liu@asu.edu (Yongming Liu)

These factors have opened up new possibilities for continuous condition monitoring of civil infrastructure at scale. In addition, autonomous inspection techniques provide an opportunity to remove subjectivity that can result from manual inspectors. While deep learning-based techniques are getting widely adopted for various types of industrial and infrastructure inspection tasks, for our experiments, we narrow the focus down to working on defect detection in structural and infrastructural systems, such as crack detection in concrete surfaces, road pavements, and pitting-corrosion and cracking defects in gas pipelines.

Accurately detecting defects within an image is a complex and challenging problem. Convolutional neural networks (CNNs) have been used to recognize and classify defects, but traditional deep learning-based models focus solely on the classification of defects and ignore underlying feature information such as crack boundaries. Detecting accurate crack boundaries is important for downstream condition monitoring and maintenance scheduling. Traditional vision-based fault detection methods use hand-crafted features that limit generalization capacity. To address this, deep learning has been used to develop more flexible and accurate models for fault detections. Given that fine-grained defect detection provides us with highly resolved defect morphology in an end-to-end fashion, the question of whether the detection is to be trusted is important. The consequences of poor detection results in a situation where the final risk assessment may be inaccurate, resulting in either a higher frequency of catastrophic events or maintenance cost overruns. To this end, the first goal of this paper is to produce uncertainty estimates along with predictions for defect detection. To do this, we make use of a sampling-based Bayesian Deep Learning approach to decompose the sources of uncertainty in prediction using the formulation proposed by Kendall and Gal (2017). Similar Bayesian Deep Learning approaches have been used in a growing number of applications (Pang et al., 2022, 2021; Lee et al., 2017). Experiments to benchmark the validity of the proposed uncertainty quantification approach are done to ensure that the characteristics needed for defect detection are met. The next goal is to formulate the defect detection problem using a multi-task loss that learns a distributional loss using the log-likelihood term, refines the boundaries of the defect, and align it to the ground truth using a boundary loss term. This formulation borrows from Wang et al. (2021) to compute a boundary loss that learns to better align predicted and ground truth boundaries. To demonstrate the effectiveness of the method, we conduct experiments on two commonly used crack segmen-

tation datasets and report results on model performance, calibration, and uncertainty for both within and out of distribution samples. To summarize, the contributions of this paper are as follows:

- We propose a Bayesian Boundary Aware Convolutional Network (B-BACN) for crack segmentation
- We use the proposed method to analyze the improvements that boundary losses can bring to improve the accuracy of the crack morphology, and we use uncertainty as a tool for analyzing model calibration.

2. Related Work

A lot of studies that focus on the defect detection problem either used classical image processing methods, that require extensive feature engineering that was prone to a lack of robustness (Liu et al., 2019a; Suvdaa et al., 2012; Liu et al., 2016; Ouma and Hahn, 2016) or used a bounding box detection approach for this problem (Yang et al., 2021; Li et al., 2021; Yin et al., 2020; Deng et al., 2021; Xu et al., 2021). Fine-grained defect detection results are crucial for any detailed morphological analysis of the structures of interest, so a bounding-box approach to this problem is not optimal. Early work in boundary refinement included applying post-processing methods such as the Conditional Random Field (CRF) based method proposed by (Krähenbühl and Koltun, 2011) and image filtering to refine crudely localized crack boundaries and then classify them using classical ML models, as seen in Shi et al. (2016). Since crack pixels are similar to edges, early works that used filters were inspired by edge detectors. However, these methods did not have semantic knowledge of the crack pixels and their relation to the background. This meant that a lot of post-processing and advanced filter design is required to remove false positives. Later works began to utilize approaches that defined boundary refinement blocks Chen et al. (2020). (Guo et al., 2021) adapts the original image gradient with the coarse crack detection result and refines it to precise crack boundaries.

Large parameter spaces in deep networks produce posteriors that are computationally intractable to integrate, and do not have pre-determined conjugate forms that make direct evaluations of updated posterior distributions possible. Due to these reasons, deep learning techniques do not lend themselves to analytical Bayesian inference and require approximate inference techniques, which have seen a lot of development in computational statistics literature

(Blei et al., 2017; Zhang et al., 2018). This paper aims to use a computationally cheap approximation to Bayesian inference in neural networks, the dropout (Srivastava et al., 2014; Gal and Ghahramani, 2016). This approach relies on producing Monte-Carlo (MC) draws from a neural network regularized by dropout to calculate a measure of dispersion in the prediction. Dropout is classically used to modulate model complexity by deactivating some parameters at random. In a Bayesian Deep Learning context, Gal and Ghahramani (2016) makes use of dropout as a model averaging tool during inference, by sampling prediction outputs from various instantiations of the neural network.

The crack detection model in our work combines uncertainty quantification and boundary refinement techniques to produce detection results that result in two main benefits: the ability to accurately segment crack morphology, and the ability to separately compute epistemic and aleatoric variances. The uncertainty is used to analyze prediction confidence and whether the model is well-trained for the test set being considered. This work also analyzes the effect that additional training samples have on uncertainty, and provides detailed empirical evaluations of within and out-of-distribution cases.

3. Methodology

Layer type	Num. filters	Filter size	Stride	Padding	Activation
ResNet-50 Backbone	-	-	-	-	-
Conv2d	1024	3	1	1	ReLU
BatchNorm2d	1024	-	-	-	-
ConvTranspose2d	512	3	2	1	ReLU
BatchNorm2d	512	-	-	-	-
ConvTranspose2d	256	3	2	1	ReLU
BatchNorm2d	256	-	-	-	-
ConvTranspose2d	128	3	2	1	ReLU
BatchNorm2d	128	-	-	-	-
Dropout	-	-	-	-	-
Conv2d	-	1	-	-	-

Table 1: Architecture details of the segmentation network

The overall architecture is based on the fully-convolutional encoder-decoder

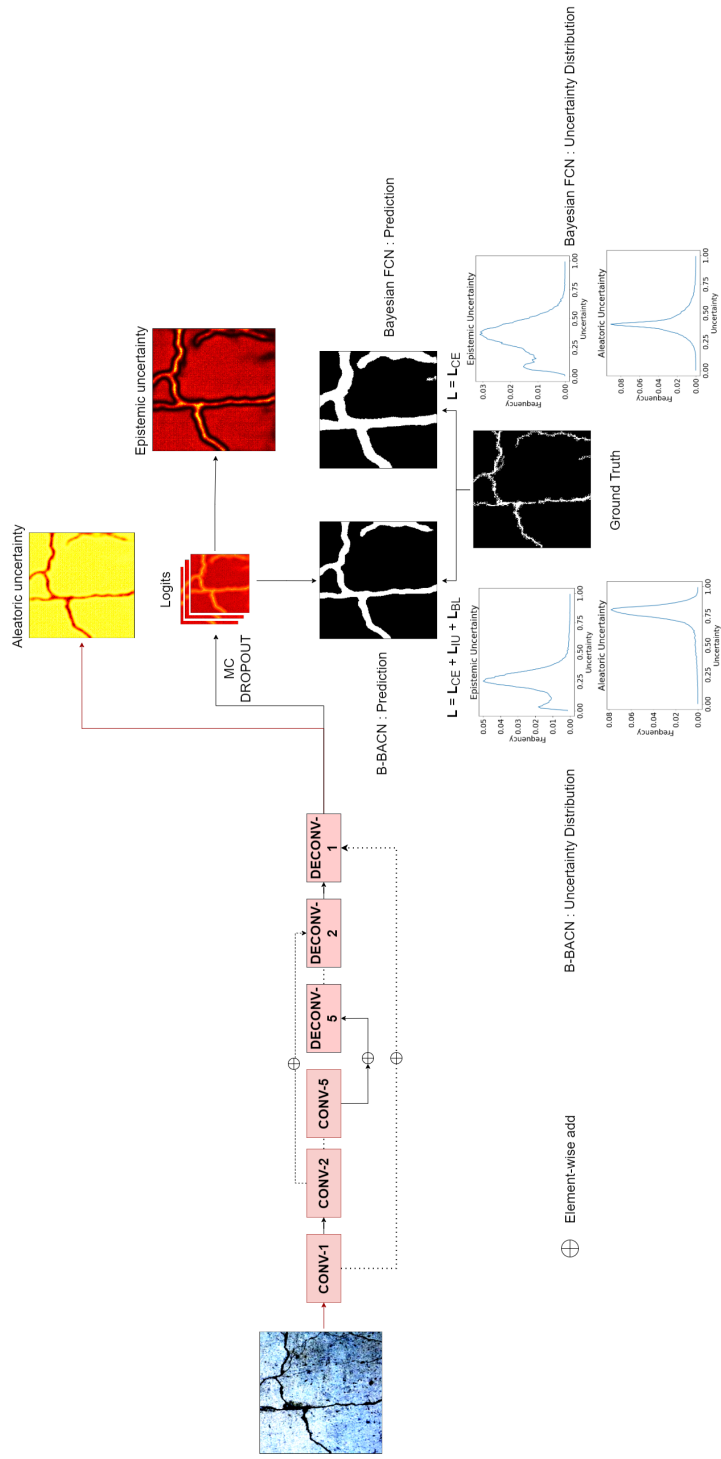


Figure 1: Overview of the proposed network architecture showing the network structure, input, predictions and uncertainty. The use of the proposed approach allows the model to predict tighter crack boundaries and epistemic uncertainties.

network (Long et al., 2017), with a Resnet-50 backbone, as shown in Figure 1, with a summary of the layers in the decoder shown in Table 1. The encoder network consists of 5 blocks, with pre-trained weights from the ImageNet dataset that are retrained for each training run. The encoder blocks provide a hierarchy of features at multiple scales, with earlier layers extracting fine-grained morphological information, and later layers extracting coarse-grained category and location information. The resulting layers are then passed into the decoder, which consists of transposed convolutions such that the feature outputs mirror the corresponding size of the next encoder layer. In addition to having information flow sequentially through each layer in the network, the skip-connections across the encoder-decoder structure combines the representations obtained across multiple scales. This approach has been successfully used in the past to help with boosting gradient flow, improving the vanishing gradient problem.

Structural prognostics benefit immensely from being able to model predictive uncertainty at multiple stages of analysis. Point estimates provided by deep neural networks may lead to overconfident predictions that can often be wrong. Ideally, we seek expressive models, have a unifying formalism to help extend the capabilities of the model for downstream tasks and have a way to explain its predictions to the end user. This is achieved by taking a Bayesian view of the problem. The Bayesian framework lends itself very well to modeling a broad range of problems, and we contend that it is easier to work with both at the level of prognostics and risk assessment and at the level of image segmentation and defect detection. In this section, we describe the Bayesian view of deep learning to evaluate predictive uncertainty for the detection task and contextualize the uncertainty within the broader framework of the prognostics pipeline. We expand upon some of the challenges in the disambiguation of uncertainties in the defect detection problem. In section 5, we empirically analyze two benchmark datasets to verify the capabilities of this approach to uncertainty quantification and then justify the importance of modeling uncertainty in an industrial informatics problem. Consider the general setup for Bayesian inference:

$$p(y^*|x^*, X, Y) = \int p(y^*|f^*)p(f^*|x^*, X, Y)df^* \quad (1)$$

In Equation 1, a prior distribution is defined over the space of functions $p(f)$ where f is a sample from the distribution of functions that could have generated the data $D = (X, Y)$. The likelihood function is $p(Y|f, X)$. The

posterior can be written using the Bayes rule from the prior $p(f)$ and the likelihood function. For an unseen data point x^* , the posterior predictive can be computed by integrating over all possible functions f^* to yield the conditional probability for prediction y^* . The problem with Equation 1 arises from the inability of neural networks to produce any meaningful uncertainty estimate as part of the prediction. While it is easy to specify conjugate distributions for simpler statistical models, it is far more challenging to obtain closed form posterior distributions for neural networks. This is because of the large dimension of the weight matrix, which leads to intractable integrals. As stated in Section 1, we use the sampling-based MC-Dropout approach to estimate the uncertainty. The dropout approach gives us insights into how it compares to other classical models. For example, when using dropout in a model trained using the mean-squared error loss function, it is equivalent in expectation to the ridge regression model. In this setup, the input feature $X \in \mathbb{R}^{N \times D}$ is to be transformed to a target $Y \in \mathbb{R}^{N \times 1}$, using weights $w \in \mathbb{R}^{D \times 1}$. Applying dropout implies multiplying the feature element-wise with a dropout mask matrix $R \sim \text{Bernoulli}(p)$. Casting this with dropout applied to the feature in the mean-squared error loss gives:

$$L(w) = \text{argmin}_w E_{(R \sim \text{Bern}(p))} \|y - (R \odot X)w\|^2 \quad (2)$$

Computing the expectation of the mean squared error loss gives us the following:

$$L(w) = \|y - X\tilde{w}\|^2 + \frac{1-p}{p} \|\Gamma\tilde{w}\|^2, \tilde{w} = p.w \quad (3)$$

Directly comparing the loss for the dropout with the ridge regression loss shows that it has stronger restrictions on its Lagrange multiplier term. Concretely, $\lambda = \frac{1-p}{p}$ for dropout, where p is the dropout probability hyperparameter, compared to the looser restriction on the multiplier for the ridge loss, $\lambda \geq 0$. Evaluating the uncertainty is done by averaging N forward passes during prediction. This is equivalent to drawing N samples from the set of parameters defined in the model posterior and evaluating a function using each of those samples. The variance of these samples ostensibly computes a form of uncertainty. Given that the desired output variable is drawn from an arbitrary distribution, the sample mean approaches the population means at large sample sizes, with a spread that is dictated by the form of the function resulting from each dropout sampling iteration. The question here is whether the uncertainty is purely derived from the uncertainty about the

weights. The analysis of the variance by Brach et al. (2020) provides some insight into this problem:

$$\begin{aligned} E_i^D &= E_i(1 - p^*) \\ V_i^D &= V_i p^*(1 - p^*) + V_i(1 - p^*)^2 + E_i^2 p^*(1 - p^*) \end{aligned} \tag{4}$$

Equation 4 shows that the expectation and variance of the output E_i^D and V_i^D only depend on the expectation E_i and variance V_i from the previous layer and the applied dropout ratio p . This shows that the only contribution to the variance in MC Dropout is from the dropout layer. Therefore, this component of uncertainty is driven by the uncertainty in the weights.

The uncertainty in the model needs to be distinguished from the uncertainty in the input data. It is possible to illustrate this distinction with the Bayesian Linear Regression model, where we decompose the uncertainty into multiple parts. As always, there is an uncertainty associated with the weights, which is expressed as part of the prior distribution. There is also inherent uncertainty in the training data distribution. This is expressed using the likelihood function of the output given the data and the parameters. The component of uncertainty that depends on the noise in the training data distribution is called the aleatoric uncertainty. Classical Bayesian linear regression formulations as seen in Bishop and Nasrabadi (2006) assume a constant, known value for this term. However, this assumption does not hold for real-world data, as some training samples can have higher variance than others. An example of this in the pipeline problem is the greater predictive uncertainty at places where occlusions and reflections that cause a degradation in the quality of the depth image. To remedy this, the model learns a component of the variance as a function of the data, referred to as the heteroscedastic aleatoric uncertainty - the component of uncertainty that cannot be explained away with more data. The epistemic component of the uncertainty is calculated using Monte Carlo (MC) dropout during inference. In the context of applying uncertainty quantification to gas pipeline risk assessment and defect detection, epistemic uncertainty plays a more important role than aleatoric uncertainty, unlike in natural image situations with a lot of data, where the aleatoric uncertainty matters more. The robotic system that has been developed can produce data that shows low variability in artifacts such as reflections and has high consistency in producing image maps without occlusions, view changes, etc. These sources of variability can be considered “input-dependent” and are captured by the heteroscedastic aleatoric

uncertainty term. On the other hand, the industrial imaging domain does not always have a lot of samples to train a model on, which requires epistemic uncertainty to reflect this. The approach used by Kendall and Gal (2017) distinguishes the epistemic and aleatoric uncertainty by deriving the loss function from the likelihood formulation. We demonstrate this approach first on a toy classification problem.

Epistemic and aleatoric uncertainty are related to the decision boundary in classification. We verify the approach on the two moons dataset, visualized in Figure 2. The two moons dataset is a non-linearly separable dataset with 2 inputs. We use the two-moons dataset because this is a low-dimensional toy problem that can be demonstrated with a large set of training samples to clarify the role of epistemic and aleatoric uncertainty. Since the model has 2 categories, the network outputs 4 values – 2 for the predictions, and 2 for each of the variances. The variance terms are the input-dependent uncertainties. For a classifier:

$$y_i|x_i \sim \text{Bern}(\psi(w^T x_i)) \quad (5)$$

Assuming softmax activation ψ , the optimal weights can be derived using Maximum Likelihood Estimation (MLE):

$$w = \text{argmax}_w p(y_i, x_i|w) \quad (6a)$$

$$w = \text{argmax}_w p(y_i|x_i, w)p(x_i|w) \quad (6b)$$

$$w = \text{argmax}_w p(y_i|x_i, w) \quad (6c)$$

Equations (6a)-(6c) lead to a stochastic negative log-likelihood loss by first setting up a Gaussian distribution to sample from. The mean of this distribution is taken as the prediction $f(x_i)^w$. The variance term comes from the learned aleatoric variance output from the network. We then sample t times from this distribution and then average its log-softmax over the sampling dimension. To avoid underflow and overflow issues, this is implemented by first transforming the $y_{i,t}$ using the log sum exp trick and then averaging over the sampling dimension. The final form of the loss is implemented directly using the *Negative Log-Likelihood (NLL)* loss, after obtaining the samples as described, and comparing the prediction against the ground truth. The loss is stochastic because it depends on Monte Carlo draws from the variance

term.

$$\begin{aligned}
 y_i|w &\sim N(f(x_i)^w, \sigma_i^{w^2}) \\
 y_{i,t} &= f(x_i)^w + \epsilon_t, \epsilon_t \sim N(0, \sigma_i^{w^2}) \\
 \mathcal{L}_{MLE} &= NLL(y_i, y_{gt})
 \end{aligned} \tag{7}$$

During the model evaluation, the procedure to compute uncertainty is by doing Monte Carlo sampling using dropout to obtain predictions. The epistemic uncertainty is computed as the variance of these predictions. The aleatoric uncertainty is the learned component of the prediction and is directly obtained from the formulation. The results in Figure 3 show that the epistemic uncertainty reduces with more training data while the aleatoric uncertainty remains oscillatory and independent of this trend. Figure 2 shows a demonstrative example of what the decision boundary looks like when using MC-Dropout. The areas with more data have a lower uncertainty in the decision boundary, indicated by the lower amount of variance in classification. At the extreme ends of the decision boundary, we notice a widening of the noise profile, indicating a higher uncertainty for the discriminative model to assign a fixed label to a sample near the boundary.

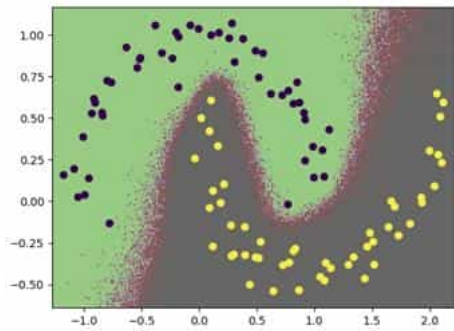


Figure 2: Classification with uncertainty in the two moons dataset - Variation of uncertainty and entropy with sample size

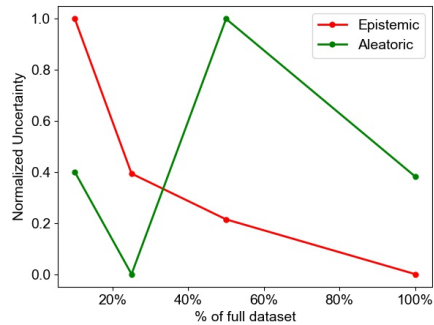


Figure 3: Classification with uncertainty in the two moons dataset - Variation of uncertainty with sample size.

The next component is the active boundary loss (ABL) that further refines predictions, proposed by (Wang et al., 2021). Since the loss is model-agnostic, we adopt it for our problem and provide a brief description of it here. This loss improves the alignment between predicted boundaries (PDBs)

and ground-truth boundaries (GTBs) during training by moving PDBs toward the closest GTBs. The ABL loss is differentiable and dynamic and it focuses on the relationship between PDB and GTB pixels. It can be used in combination with other loss terms such as cross-entropy loss and Lovasz-softmax loss to improve the boundary details in image segmentation. The method can be useful in preserving the boundaries of thin objects in an image. The ABL continuously monitors changes in the PDBs to determine the plausible moving directions. The method is divided into two phases: First, for each pixel i on the PDBs, the next candidate boundary pixel j closest to the GTBs is determined. Second, the KL divergence is used to encourage the increase in KL divergence between the class probability distribution of i and j . Meanwhile, this process reduces the KL divergence between i and the rest of its neighboring pixels. In this way, the PDBs can be gradually pushed toward the GTBs. Unfortunately, conflicts might occur and the performance of the ABL can degrade, so the authors use gradient flow control to reduce the conflicts. The details of this process are elaborated in (Wang et al., 2021). We also use the Jaccard loss, given by the Lovasz-softmax function (Berman et al., 2017), to refine the regional shape of the detected crack by directly optimizing for higher Intersection-over-Union (IoU) score.

Additionally, we perform temperature scaling on the logits to calibrate the predicted probability distributions of the network, following Guo et al. (2017), where the temperature is a learnable hyperparameter (T). We compute the temperature by using the validation set, by choosing the temperature that minimizes the negative log-likelihood of the model.

In summary, the overall proposed loss is the combination of the derived heteroscedastic classification loss, the IoU loss and the ABL loss:

$$L = L_{MLE} + L_{ABL} + L_{IOU} \quad (8)$$

4. Experimental Setup

4.1. Implementation Details

The experiments are performed on the CrackForest dataset by Shi et al. (2016) and DeepCrack dataset (Liu et al., 2019b). The CrackForest dataset is representative of a variety of cracks encountered in urban roads, and has been used as a benchmark for multiple studies such as Shi et al. (2016), Fan et al. (2018), Yang et al. (2019), Zou et al. (2018). It consists of 100 images, with 18 left out for the test set. The DeepCrack dataset is a larger

dataset consisting of crack images at multiple scales and background textures. It consists of 443 training set images and 78 test set images. The network architecture used for the main experiments is the Resnet50 backbone encoder with a transposed convolutional decoder, as explained in Section 3, and the models are trained using PyTorch. The training code has the ability to run in both single and multi GPU configurations, with our training using a single NVIDIA 1080Ti GPU that has 11 GB of VRAM. The encoder uses a set of pre-trained weights from the ImageNet dataset, which is then fully retrained using the specific dataset for the experiment. We employ the use of the SGD with momentum optimizer, with a momentum value of 0.9 and weight decay of 10^{-5} , along with a step-decay learning rate scheduler across our experiments. For the initial learning rate, we start at 0.01, which decays every 50 epochs by a factor of 0.8. During training, we also implement early stopping based on the validation loss history over the past 50 epochs. The early stop condition used for our experiments is an average validation loss reduction of less than 0.001. For the experiments across training samples, a dropout probability of 0.5 was used. We extract the epistemic uncertainty during model evaluation using 25 Monte-Carlo runs through the network. To quantify model performance, we make use of the macro F-1 score to report the mean F-1 score, which is an unweighted average of the class-wise F-1 scores.

4.2. Evaluation Metrics

To quantify model performance, we make use of the macro F-1 score to report the mean F-1 score, which is an unweighted average of the class-wise F-1 scores. The F-1 score is defined as the harmonic mean of precision and recall, and typically used to measure how well the segmentation captures crack morphology. The equation for the F-1 score is:

$$F_1 = \frac{2 \cdot Precision \cdot Recall}{Precision + Recall} \quad (9)$$

We also compute the entropy and variance of the predictions over 25 Monte-Carlo runs to assess the level of uncertainty in the model out of those samples. To quantify the model’s calibration, we make use of the Expected Calibration Error (ECE) (Guo et al., 2017) (Naeini et al., 2015), using 30 bins to measure the difference between the calibration score and the reliability. The ECE is computed using Eq. 10, with the calibration bin accuracy $Acc(B_m)$ and the

overall accuracy of the class m

$$ECE = \sum_{m=1}^M \frac{|B_m|}{n} |acc(B_m) - conf(B_m)| \quad (10)$$

5. Results and Discussion

In our experiments, we first show the performance of the model using the baseline MC-Dropout model, the B-BACN model and the Temperature-Scaled B-BACN model on the DeepCrack dataset and the CrackForest datasets, establishing that the proposed B-BACN model significantly improves the detection performance, while reducing uncertainty and improving the expected calibration error. Adding temperature scaling does not provide further improvements. The technique used for modeling uncertainty, as demonstrated in Section 3, aims to capture specific behaviors of uncertainty, such as detecting higher uncertainty when the test samples are farther from the training samples and having an invariant aleatoric component with respect to the training samples. Therefore, we demonstrate model performance across training samples and dropout, revealing the utility of uncertainty metrics for determining whether the model is well-trained and to what extent these trends seen on the simpler two-moons dataset hold for the segmentation dataset. We then demonstrate how the uncertainty model generalizes to unseen and out-of-distribution data samples from the CrackForest dataset. Since the DeepCrack dataset is out of the distribution of the CrackForest dataset, we expect the epistemic entropy to increase for these samples. Additionally, we show that the aleatoric component of uncertainty does not decrease despite training on the CrackForest dataset. We also present the performance of our model on a smaller CrackForest dataset, trained with noisy data, with and without the introduction of the boundary loss. We evaluate the model’s performance quantitatively using metrics such as the F1 score, as well as qualitatively by using demonstrative detection results and uncertainty maps.

The first set of results compares model performance on the DeepCrack test set using the boundary loss against the MC Dropout baseline. Not only does the boundary loss exceed F1 score compared to the baseline, but also shows a drop in the variance of the prediction. The models used were trained on the DeepCrack dataset using all the available training data. These results indicate that using the boundary loss terms helps to directly operate on and

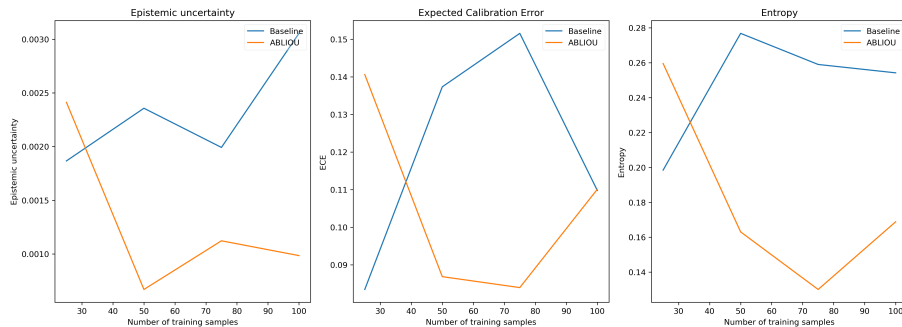


Figure 4: Uncertainty across training samples for the CrackForest Dataset for (a) Cross-Entropy trained Bayesian FCN (Baseline) (b) Proposed B-BACN with the ABL-IOU loss (ABLIOU)

refine the pixel-level predictions. Table 2 shows these results, and Figure 6 provides some demonstrative detection examples that compare these results. Similar trends are observed for the CrackForest dataset. The predicted boundary changes were also compared between the boundary loss model and the cross entropy model, with the boundary loss model providing more accurate boundaries and lower uncertainty compared to the baseline.

Evaluating the model across various training samples shows a trend similar to the one seen in the toy problem in Section 3. We plot these results in Figure 4 and Figure 5. The epistemic uncertainty showed a rather jagged trend for the baseline cross-entropy trained model, but showed a stronger decreasing trend for the B-BACN. This result was somewhat surprising as we expect there to be an approximately inverse relationship between the amount of training data and the uncertainty. Given enough training samples, more information does not meaningfully change the uncertainty. (Chen et al., 2010) shows that the result holds true only for normally distributed variables, and that the relationship between the uncertainty and information is not straightforward in other cases. The level of uncertainty is higher on the out-of-distribution DeepCrack dataset while the aleatoric uncertainty, as expected, does not change much. The calibration error is also higher in the out-of-distribution dataset, and adding more training samples from the CrackForest dataset does not improve this.

Analyzing the models with various dropout ratios reveals the effect of modifying this important hyperparameter. Increasing dropout was expected to make the model less prone to overfit but also increase the prediction variance

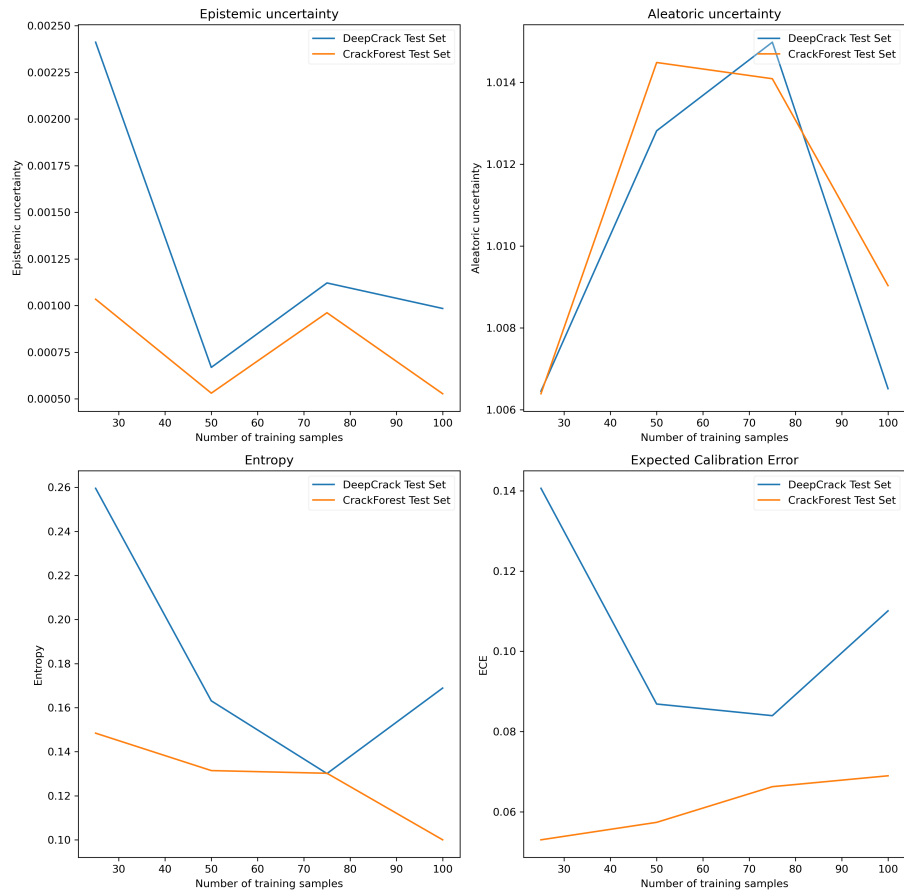


Figure 5: Uncertainty across training samples for a model trained on the CrackForest dataset: (a) CrackForest test set (b) DeepCrack test set

- This expectation bore out across both the baseline MC Dropout model, and the B-BACN. We also observe a consistent pattern of lower uncertainty, better calibration, and higher predictive performance across dropout ratios for the B-BACN model, as shown in Figure 8.

We end the results section by providing a more detailed demonstration of model calibration using the model trained on the DeepCrack dataset. To do this, we first assessed the calibration on the DeepCrack test set, then evaluated the model’s performance on the CrackForest test set. which contains out-of-distribution examples. Finally, we tested the model’s robustness by introducing noise to the CrackForest test set to simulate a challenging scenario. One of the main objectives of predictive models is to ensure that a higher level of uncertainty is assigned to labels that deviate from the ground truth assignment, which can be verified in the validation set as the ground truth is available during the evaluation process. Figure 7 illustrates how the class-wise model uncertainty score aligns with the prediction quality, which is quantified by the class-wise F1 score. The points should be close to the line of equality (LOE) as shown in green, or demonstrate a negative correlation to uncertainty, which indicates that there is increasing uncertainty for samples that have a poor detection score in the test set. The first row of Figure 7 demonstrates that the DeepCrack background data is very well calibrated, but the crack class is less calibrated. However, the calibration performance worsens with the out-of-distribution data in row 2. In row 3, however, we add Gaussian noise with a mean of 0 and a variance between 10 and 50. Introducing such high levels of noise shows the strong effect that it has on the model calibration. Model calibration methods such as the one shown in this study can therefore be used along with the expected calibration error to obtain more detailed evaluations of the image quality.

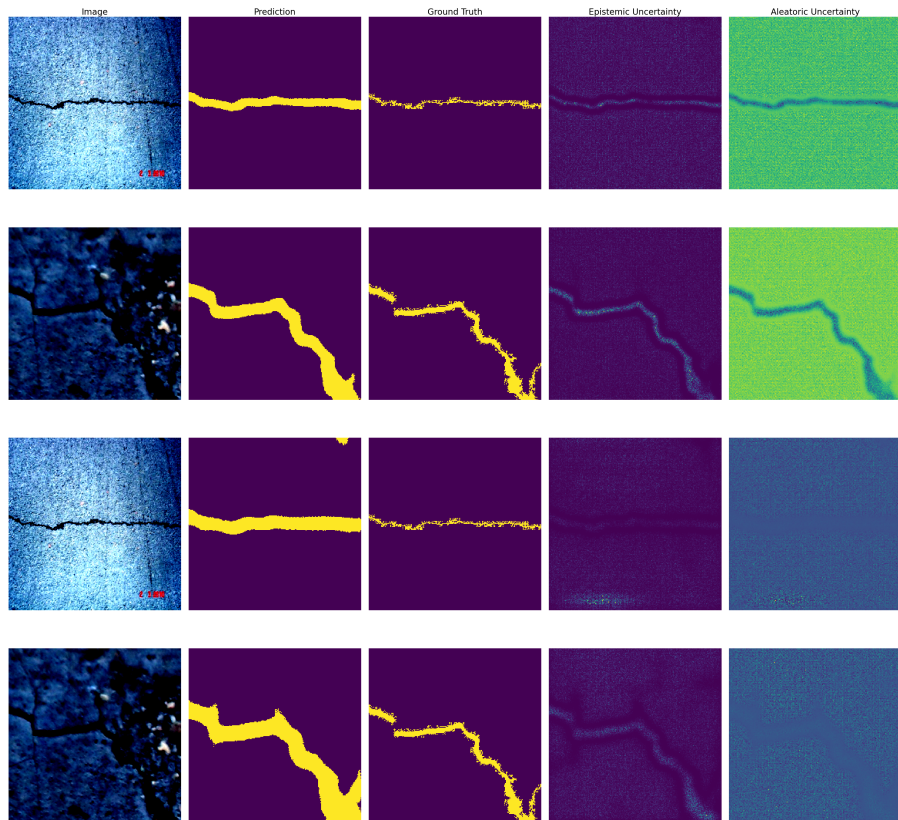


Figure 6: Demonstrative examples of detections in the CrackForest (Top-2 rows) and the DeepCrack Dataset (Bottom-2 rows). Images from Left to Right: Input, Prediction, Ground Truth, Epistemic Uncertainty, Aleatoric Uncertainty

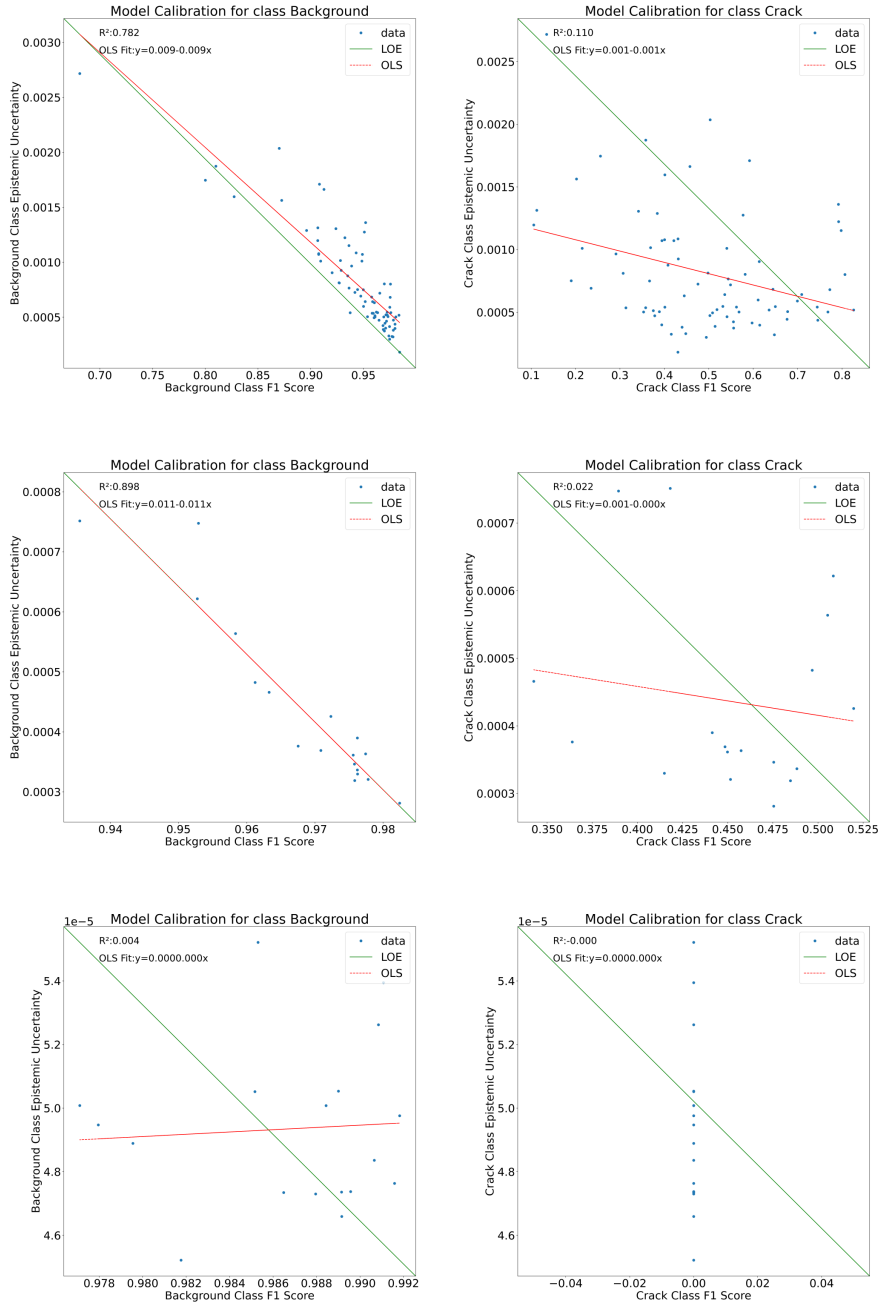


Figure 7: Model Calibration Plot for a model trained on the DeepCrack dataset : (Top row) Evaluation on the DeepCrack test set (Middle row) Evaluation on the CrackForest test set (Bottom row) Evaluation on a noisy CrackForest test set

Table 2: Performance comparison for models trained on DeepCrack and CrackForest dataset: MC Dropout, MC Dropout with Boundary Loss and Temperature Scaling

Dataset	Model	F1	Epistemic	Aleatoric	ECE
DeepCrack	MC Dropout	0.70890	0.000314	1.021434	0.146566
DeepCrack	Boundary Loss + IOU (BL + IOU)	0.800602	0.000190	1.031051	0.103713
DeepCrack	Temperature Scaled BL + IOU	0.638598	0.000534	1.036237	0.099453
CFD	MC Dropout	0.698819	0.000218	1.013456	0.076171
CFD	Boundary Loss + IOU (BL + IOU)	0.795779	0.000195	1.019214	0.090102
CFD	Temperature Scaled BL + IOU	0.746244	0.000153	1.018989	0.033556

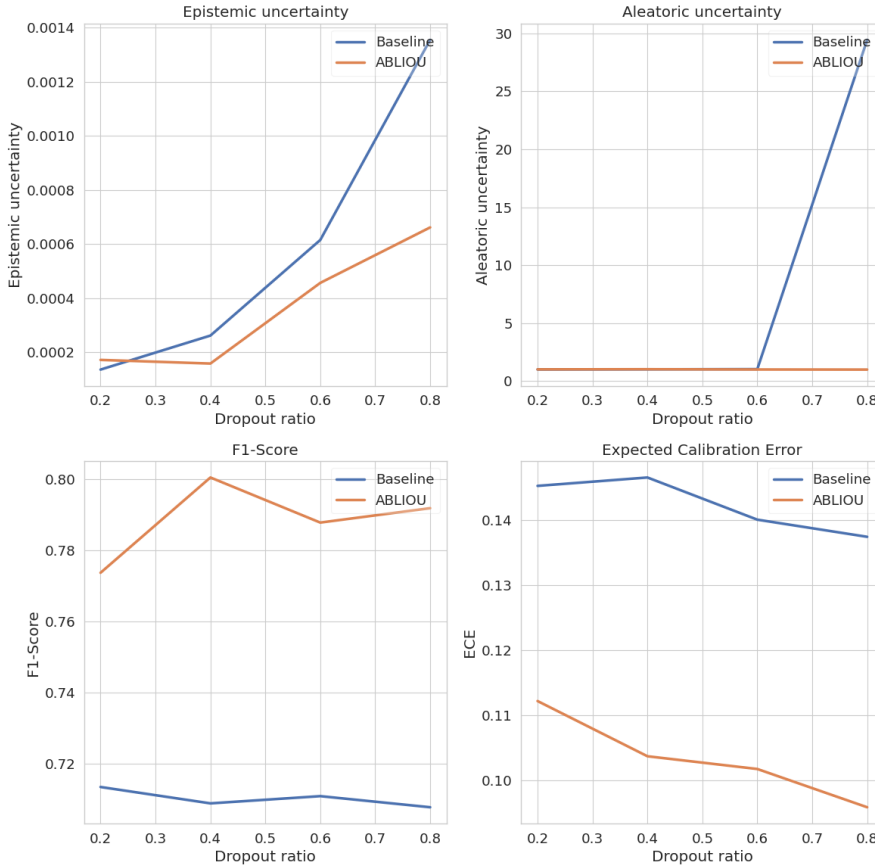


Figure 8: Uncertainty, F1 score and calibration error on the DeepCrack test set across dropout ratios: (a) Epistemic uncertainty and (b) F1 score (c) Expected Calibration Error

6. Conclusion

In this paper, we have presented the Bayesian-Boundary Aware Convolutional Network (B-BACN), which decomposes the uncertainty into an epistemic and an aleatoric component, along with a boundary refinement loss that further improves crack morphology. The proposed B-BACN model significantly improves the detection performance, while reducing uncertainty and improving the expected calibration error, compared to the baseline. The use of boundary loss functions can therefore not only aid in improved test performance by refining pixel-level predictions, but also help in reducing model size. The knowledge of uncertainty formulation would aid inspection protocols by providing indicators of distribution shift and lack of training data. To test this, the proposed uncertainty formulation was used to study the epistemic and aleatoric uncertainty when the test data moves further away from the training distribution. While we saw an increase in the model uncertainty and a decrease in model calibration with out-of-distribution samples, we also obtained empirical evidence for a more complicated relationship between the uncertainty obtained from sampling, the amount of training data present, and the inherent uncertainty in the data that was predicted by the model. This observation can help guide future studies to provide more empirical evidence on this relationship and extend existing theoretical work on the problem.

7. Acknowledgement

This work was supported by the Competitive Academic Agreement Program (CAAP) of the Pipeline and Hazardous Materials Safety Administration (PHMSA) which is a part of the US Department of Transportation. The CAAP project contract ID number is 693JK31950002CAAP.

References

- Berman, M., Triki, A.R., Blaschko, M.B., 2017. The lovász-softmax loss: A tractable surrogate for the optimization of the intersection-over-union measure in neural networks. URL: <https://arxiv.org/abs/1705.08790>, doi:10.48550/ARXIV.1705.08790.
- Bishop, C.M., Nasrabadi, N.M., 2006. Pattern recognition and machine learning. volume 4. Springer. URL: <https://dl.acm.org/doi/10.5555/1162264>.

- Blei, D.M., Kucukelbir, A., McAuliffe, J.D., 2017. Variational inference: A review for statisticians. *Journal of the American statistical Association* 112, 859–877. doi:<https://doi.org/10.1080/01621459.2017.1285773>.
- Brach, K., Sick, B., Dürr, O., 2020. Single shot mc dropout approximation. arXiv preprint doi:[arXiv:2007.03293](https://arxiv.org/abs/2007.03293).
- Chen, J., van Eeden, C., Zidek, J., 2010. Uncertainty and the conditional variance. *Statistics and Probability Letters* 80, 1764–1770. URL: <https://www.sciencedirect.com/science/article/pii/S0167715210002154>, doi:<https://doi.org/10.1016/j.spl.2010.07.021>.
- Chen, X., Lian, Y., Jiao, L., Wang, H., Gao, Y., Lingling, S., 2020. Supervised edge attention network for accurate image instance segmentation, in: *European Conference on Computer Vision*, Springer. pp. 617–631.
- Deng, J., Lu, Y., Lee, V.C.S., 2021. Imaging-based crack detection on concrete surfaces using you only look once network. *Structural Health Monitoring* 20, 484–499. doi:<https://doi.org/10.1177/1475921720938486>.
- Fan, Z., Wu, Y., Lu, J., Li, W., 2018. Automatic pavement crack detection based on structured prediction with the convolutional neural network. arXiv preprint doi:[arXiv:1802.02208](https://arxiv.org/abs/1802.02208).
- Gal, Y., Ghahramani, Z., 2016. Dropout as a bayesian approximation: Representing model uncertainty in deep learning, in: *international conference on machine learning*, PMLR. pp. 1050–1059. URL: <https://proceedings.mlr.press/v48/gal16.html>.
- Guo, C., Pleiss, G., Sun, Y., Weinberger, K.Q., 2017. On calibration of modern neural networks. URL: <https://arxiv.org/abs/1706.04599>, doi:[10.48550/ARXIV.1706.04599](https://doi.org/10.48550/ARXIV.1706.04599).
- Guo, J.M., Markoni, H., Lee, J.D., 2021. Barnet: Boundary aware refinement network for crack detection. *IEEE Transactions on Intelligent Transportation Systems* .
- Kendall, A., Gal, Y., 2017. What uncertainties do we need in bayesian deep learning for computer vision? *CoRR* abs/1703.04977. doi:[arXiv:1703.04977](https://arxiv.org/abs/1703.04977).

- Krähenbühl, P., Koltun, V., 2011. Efficient inference in fully connected crfs with gaussian edge potentials. *Advances in neural information processing systems* 24.
- Lee, J.G., Jun, S., Cho, Y.W., Lee, H., Kim, G.B., Seo, J.B., Kim, N., 2017. Deep learning in medical imaging: general overview. *Korean journal of radiology* 18, 570–584. doi:10.3348/kjr.2017.18.4.570.
- Li, D., Xie, Q., Yu, Z., Wu, Q., Zhou, J., Wang, J., 2021. Sewer pipe defect detection via deep learning with local and global feature fusion. *Automation in Construction* 129, 103823. doi:<https://doi.org/10.1016/j.autcon.2021.103823>.
- Liu, M., Liu, Y., Hu, H., Nie, L., 2016. Genetic algorithm and mathematical morphology based binarization method for strip steel defect image with non-uniform illumination. *Journal of Visual Communication and Image Representation* doi:10.1016/j.jvcir.2015.04.005.
- Liu, Y., Xu, K., Xu, J., 2019a. An improved MB-LBP defect recognition approach for the surface of steel plates. *Applied Sciences (Switzerland)* doi:10.3390/app9204222.
- Liu, Y., Yao, J., Lu, X., Xie, R., Li, L., 2019b. Deepcrack: A deep hierarchical feature learning architecture for crack segmentation. *Neurocomputing* 338, 139–153. URL: <https://www.sciencedirect.com/science/article/pii/S0925231219300566>, doi:<https://doi.org/10.1016/j.neucom.2019.01.036>.
- Long, J., Shelhamer, E., Darrell, T., 2017. Fully convolutional networks for semantic segmentation. *IEEE Transactions on Pattern Analysis and Machine Intelligence* doi:10.1109/TPAMI.2016.2572683.
- Naeini, M.P., Cooper, G., Hauskrecht, M., 2015. Obtaining well calibrated probabilities using bayesian binning, in: *Proceedings of the AAAI conference on artificial intelligence*.
- Ouma, Y.O., Hahn, M., 2016. Wavelet-morphology based detection of incipient linear cracks in asphalt pavements from rgb camera imagery and classification using circular radon transform. *Advanced Engineering Informatics* 30, 481–499. URL: <https://www.sciencedirect.com/science/article/pii/S1538851816300000>.

com/science/article/pii/S1474034616301598, doi:<https://doi.org/10.1016/j.aei.2016.06.003>.

- Pang, Y., Zhao, X., Hu, J., Yan, H., Liu, Y., 2022. Bayesian spatio-temporal graph transformer network (b-star) for multi-aircraft trajectory prediction. *Knowledge-Based Systems* , 108998doi:<https://doi.org/10.1016/j.knosys.2022.108998>.
- Pang, Y., Zhao, X., Yan, H., Liu, Y., 2021. Data-driven trajectory prediction with weather uncertainties: A bayesian deep learning approach. *Transportation Research Part C: Emerging Technologies* 130, 103326. doi:<https://doi.org/10.1016/j.trc.2021.103326>.
- Shi, Y., Cui, L., Qi, Z., Meng, F., Chen, Z., 2016. Automatic road crack detection using random structured forests. *IEEE Transactions on Intelligent Transportation Systems* doi:10.1109/TITS.2016.2552248.
- Srivastava, N., Hinton, G., Krizhevsky, A., Sutskever, I., Salakhutdinov, R., 2014. Dropout: a simple way to prevent neural networks from overfitting. *The journal of machine learning research* 15, 1929–1958. URL: <http://jmlr.org/papers/v15/srivastava14a.html>.
- Suvdaa, B., Ahn, J., Ko, J., 2012. Steel surface defects detection and classification using SIFT and voting strategy. *International Journal of Software Engineering and its Applications* doi:10.1.1.375.7366.
- Wang, C., Zhang, Y., Cui, M., Liu, J., Ren, P., Yang, Y., Xie, X., Hua, X., Bao, H., Xu, W., 2021. Active boundary loss for semantic segmentation. *CoRR abs/2102.02696*. URL: <https://arxiv.org/abs/2102.02696>, arXiv:2102.02696.
- Xu, Y., Li, D., Xie, Q., Wu, Q., Wang, J., 2021. Automatic defect detection and segmentation of tunnel surface using modified mask r-cnn. *Measurement* 178, 109316. doi:<https://doi.org/10.1016/j.measurement.2021.109316>.
- Yang, D., Cui, Y., Yu, Z., Yuan, H., 2021. Deep learning based steel pipe weld defect detection. *Applied Artificial Intelligence* , 1–13doi:<https://doi.org/10.1080/08839514.2021.1975391>.

- Yang, F., Zhang, L., Yu, S., Prokhorov, D., Mei, X., Ling, H., 2019. Feature pyramid and hierarchical boosting network for pavement crack detection. *IEEE Transactions on Intelligent Transportation Systems* 21, 1525–1535. doi:10.1109/TITS.2019.2910595.
- Yin, X., Chen, Y., Bouferguene, A., Zaman, H., Al-Hussein, M., Kurach, L., 2020. A deep learning-based framework for an automated defect detection system for sewer pipes. *Automation in construction* 109, 102967. doi:<https://doi.org/10.1016/j.autcon.2019.102967>.
- Zhang, C., Bütepage, J., Kjellström, H., Mandt, S., 2018. Advances in variational inference. *IEEE transactions on pattern analysis and machine intelligence* 41, 2008–2026. doi:10.1109/TPAMI.2018.2889774.
- Zou, Q., Zhang, Z., Li, Q., Qi, X., Wang, Q., Wang, S., 2018. Deepcrack: Learning hierarchical convolutional features for crack detection. *IEEE Transactions on Image Processing* 28, 1498–1512. doi:10.1109/TIP.2018.2878966.